Nanoscale

Accepted Manuscript

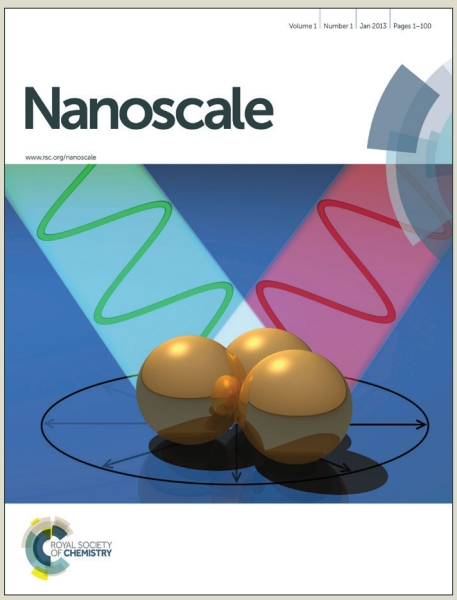

ROYAL SOCIETY OF CHEMISTRY

www.rsc.org/nanoscale

Nanoscale

RSCPublishing

ARTICLE

Epitaxial 1D Electron Transport Layers for High-Performance Perovskite Solar Cells

Cite this: DOI: 10.1039/xoxxooooox

Gill Sang Han,[a,b] Hyun Suk Chung,[a] Dong Hoe Kim,[c] Byeong Jo Kim,[a] Jin Wook Lee,[d] Nam-Gyu Park,[d] In Sun Cho,[e] Jung-Kun Lee,[b] Sangwook Lee,[f]* and Hyun Suk Jung[a]*

Received ooth January 2015,
Accepted ooth January 2015

DOI: 10.1039/xoxxooooox

www.rsc.org/

We demonstrate high-performance perovskite solar cells with excellent electron transport properties using a one-dimensional (1D) electron transport layer (ETL). The 1D array-based ETL is comprised of 1D SnO_2 nanowires (NWs) array grown on a F:SnO_2 transparent conducting oxide substrate and rutile TiO_2 nanoshells epitaxially grown on the surface of the 1D SnO_2 NWs. The optimized devices show more than 95% internal quantum yield at 750 nm, and a power conversion efficiency (PCE) of 14.2%. The high quantum yield is attributed to dramatically enhanced electron transport in the epitaxial TiO_2 layer, compared to that in conventional nanoparticle-based mesoporous TiO_2 (mp-TiO_2) layers. In addition, the open space in the 1D array-based ETL increases the prevalence of uniform TiO_2/perovskite junctions, leading to reproducible device performance with a high fill factor. This work offers a method to achieve reproducible, high-efficiency perovskite solar cells with high-speed electron transport.

Introduction

Emerging perovskite solar cells, using organometallic halides with perovskite crystal structures as light-absorbing materials, attract great attention for their continuous renewal of world-record power conversion efficiency (PCE) achievements, as well as for the economically viable processes for their fabrication.[1,2] Recent high-PCE perovskite solar cells have n-i-p junction structures mainly comprising a hole transport layer (HTL; spiro-OMeTAD or poly-triarylamine, representatively),[3,4] perovskite light-absorbing layer ($CH_3NH_3PbX_{3-x}X'_x$, where X = I, and X' = Cl or Br),[5,6] and electron transport layer (ETL; TiO_2 or ZnO, representatively).[7-10] The highest PCE reported from this type of perovskite solar cell is 20.2%.[11]

The n-i-p junction-type perovskite solar cells can be classified by their ETL structures: pillared structures with $CH_3NH_3PbI_3$, and planar structures with $CH_3NH_3PbI_{3-x}Cl_x$, depending on the charge-transport ability of the light-absorbing materials.[12] Usually, oxide nanoparticle (NP)-based mesoporous (mp) layers are used for the ETL of pillared structures. The main reason for using the mp-ETL is the short electron diffusion length (L_n) ~ 100 nm of $CH_3NH_3PbI_3$, of which film thickness is not sufficient for the full absorption of incident solar light. Therefore, the electron transport ability of the mp-ETL is very important in the pillared structure cells, to redeem the poor electron transport property of LAL. The mp-ETL plays two other roles: an extractor of electrons from the perovskite layer and a scaffolding to support the large volume of the perovskite layer. To optimize these two roles, all the pores in the mp-ETL layer should be filled with perovskite material, otherwise the device performance would be degraded by low shunt resistance due to the direct contact of the ETL and HTL, large series resistance of the device due to longer electron/hole path,[13-15] recombination at the exposed surfaces of the ETL and light absorbing perovskite layer, and low amount of perovskite materials.[13,16] However, it is very hard to perfectly fill the labyrinthine pore network of the mp-ETL.[17]

From this perspective, a single-crystalline or highly oriented 1D array-based ETL (1D-ETL) is promising because of its excellent charge transport properties and open-pore structure, in contrast with those of conventional mp-ETLs.[8-10,17-19] A recent work reported 1D ZnO-ETL-based perovskite solar cells in which relatively sparsely packed ZnO nanowires (NWs) with small diameter (24.1 nm) and length (600 nm) are employed.[8] This thin and short ZnO NWs-based perovskite solar cells exhibit higher PCE, 14.35%,[8] than the former large-size 1D ZnO-based perovskite solar cells (PCE < 12%).[7,18,20,21] On the other hand, 1D TiO_2-ETL-based perovskite solar cells show lower PCE (13.45%,[22] the best) than the recent 1D ZnO-based devices, although reverse in the mp-ETL-based perovskite solar cells; the best PCE for mp-TiO_2 is 20.2%,[11] while that of mp-ZnO is 15.7%.[23] This inconsistency is understood to result from insufficient light absorption, owing to densely packed large-

diameter 1D TiO_2,[17,22,24-27] which might reduce the available space for light-absorbing material. In case of single-crystalline TiO_2 nanowires (NWs) grown on conductive substrates, it seems so far difficult to simultaneously have a low packing density, and small diameter (a few tens of nm) and length (a few hundreds of nm), in spite of a number of works on it.[28-32]

In this work, we demonstrate a high-PCE (14.2%) perovskite solar cell based on 1D-ETL structures, comprising TiO_2 nanoshell/SnO_2 NWs. Single-crystalline rutile-structured SnO_2 NWs were grown on a F:SnO_2 (FTO) transparent conducting oxide (TCO) substrate via a vapor-liquid-solid (VLS) reaction, and TiO_2 nanoshells were epitaxially grown on the surface of the SnO_2 NWs via plasma-enhanced atomic layer deposition (PEALD). Owing to the ultrathin (20 nm) and short (300 nm) SnO_2 NWs, the SnO_2/FTO shows nearly the same transmittance as bare FTO for all wavelengths. Optimized TiO_2/SnO_2 NW-based perovskite solar cells exhibit more than 95% absorbed photon-to-current conversion efficiency (APCE) at 750 nm, and an electron transport time one order of magnitude smaller than that of mp-ETL-based devices, which are attributed to the epitaxial rutile TiO_2 nanoshell. In addition, we observed that perovskite uniformly fills the pores of the TiO_2/SnO_2 NW-based ETL, which may correlate to higher mean values and a narrower distribution of fill factors in TiO_2/SnO_2 NW-based devices compared to in mp-TiO_2-based devices.

Results and Discussion

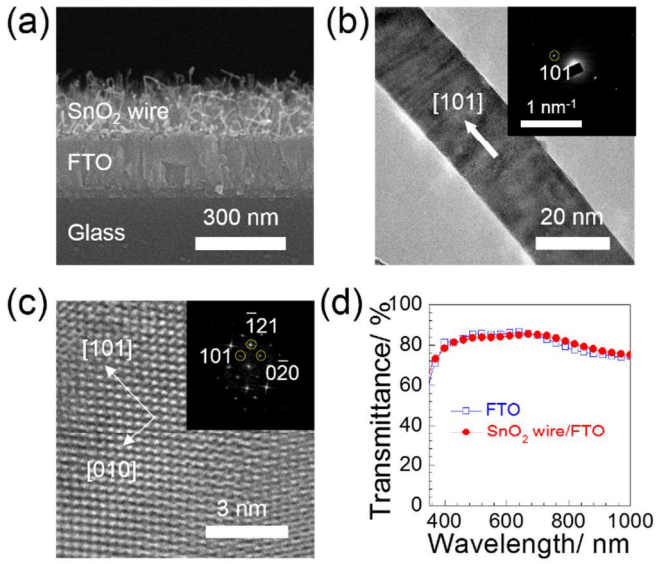

Figure 1. (a) Cross-sectional FE-SEM image of synthesized SnO_2 NWs arrays on FTO substrate. (b) TEM image of a typical SnO_2 NW (inset: SAED pattern). (c) High-resolution TEM (HRTEM) lattice image of the SnO_2 NW with [-101] zone axis (inset: FFT pattern), and (d) UV-vis transmittance spectrum for bare FTO and SnO_2 NW/FTO.

Figure 1a and **1b** show microstructure of the synthesized SnO_2 NWs, taken with a field-emission scanning electron microscope (FESEM) and a transmission electron microscope (TEM). NWs are compactly grown on the FTO substrate. Most of the NWs possess a small degree of kinked features, and are mostly straight, typical of VLS-grown SnO_2 NWs.[33,34] The length and diameter of the SnO_2 NWs can be controlled from 100 to 2000 nm and from 5 to 20 nm, respectively, by adjusting the reaction time, temperature, and oxygen flow rate. The optimized length and thickness were found to be 300 nm and 20 nm, respectively, for application in perovskite solar cells. The axial direction, i.e., its longitudinal direction, is [101] of rutile structure as shown in **Figure 1b** and **1c**, consistent with the preferred crystal growth direction of rutile SnO_2.[35,36] Although some kinked NWs and non-uniform contrasts appear in the NWs, the selected-area electron diffraction (SAED) patterns obtained from many other places show the same axial direction of rutile [101], indicating the single-crystallinity of the SnO_2 NWs. **Figure 1d** shows the UV/vis transmittance spectra of bare FTO and SnO_2 NWs/FTO. Notably, the bare FTO substrate and the SnO_2 NW/FTO exhibit similar transmittance at over 400 nm of wavelength, which can be attributed to the large band gap of SnO_2 (3.7 eV) and the sparse packed, thin and short NWs.

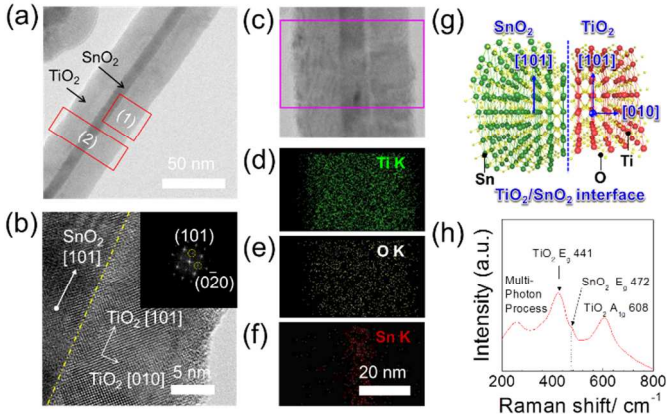

Figure 2. (a) TEM image of a typical TiO_2 nanoshell-coated SnO_2 NW, and (b) HRTEM lattice image showing the SnO_2 NW/TiO_2 interface (inset: FFT pattern). (c-f) STEM image of the TiO_2 nanoshell-coated SnO_2 NW, and elemental maps for Ti, O, and Sn, respectively. (g) Illustration of epitaxial TiO_2 on SnO_2. (h) Raman shift spectrum showing three active modes for rutile TiO_2: multi-proton process (240 cm^{-1}), Eg (441 cm^{-1}), and A_{1g} (608 cm^{-1}).[37]

Figure 2a and **2b** show the morphology and lattice image of the TiO_2 nanoshell-coated SnO_2 NWs. TiO_2 layers deposited via ALD show smooth surfaces, uniform thicknesses and no cracks. The thickness of the TiO_2 nanoshell is tunable by the number of deposition cycles, with a deposition rate of 0.5 Å per cycle. The device performance was optimal with a 20 nm-thick TiO_2 nanoshell. **Figure 2c-f** shows scanning transmission electron microscopy (STEM) images and elemental mapping of Ti, O, and Sn, which clearly show the SnO_2 core and TiO_2 shell. The crystal structure of the TiO_2 nanoshell is rutile, confirmed by Raman spectroscopy (**Figure 2h**) and SAED (**Figure 2b** inset) analyses. Substrate-dependent phase formation in ALD-grown TiO_2 has been reported frequently. For example, we reported the formation of the anatase phase on ITO NWs using the same process,[9] while other groups observed rutile phase on rutile substrates with similar lattice parameters, such as SnO_2 and RuO_2, as the nucleation of the rutile phase can be more energetically stable than that of the anatase phase.[38-41]

Interestingly, the fast Fourier transformed (FFT) patterns show exact matches in crystal directions of the TiO_2 nanoshell and the SnO_2 core. The HRTEM lattice image obtained from the TiO_2/SnO_2 interface (**Figure 2b**) also shows continuous lattice fringes across the interface. Both the SnO_2 core and TiO_2 shell have (101) planes parallel to the axial direction, and (010) planes aligned radially. This confirms the epitaxial formation of the TiO_2 shell as illustrated in **Figure 2g**.

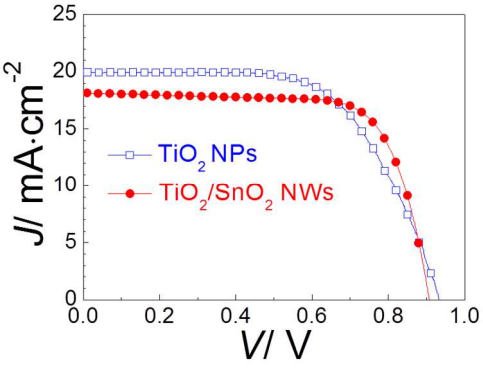

Figure 3. *J-V* curves of TiO_2 NP-based mp-ETL and TiO_2/SnO_2 NW-based 1D-ETL perovskite solar cells.

	J_{sc} (mA/cm^2)	V_{oc} (V)	*FF*	η (%)
TiO_2 NPs	19.8±1.5	0.900±0.041	0.62±0.06	11.1±1.2
TiO_2/ SnO_2 NWs	18.6±1.6	0.906±0.064	0.70±0.05	11.9±1.5

Table 1. Mean values of photovoltaic properties of TiO_2/SnO_2 NW-based 1D-ETL and TiO_2 NP-based mp-ETL perovskite solar cells.

Figure 3a shows typical *J-V* curves of the TiO_2/SnO_2 NWs-based 1D-ETL perovskite solar cells and TiO_2 NP-based mp-ETL cells. The mean values of the short circuit current density (J_{sc}), open circuit voltage (V_{oc}), fill factor (*FF*), and PCE of the 1D-ETL devices (34 devices) and mp-ETL devices (38 devices) are summarized in **Table 1**; statistical data are shown in **Figure S1,** ESI†. The 1D-ETL cells' device characteristics differ significantly from those of the mp-ETL cells, although both types exhibit similar PCE. The 1D-ETL cells show slightly lower J_{sc}, but significantly higher *FF* than the mp-ETL cells. In addition, facile pore-filling seems to improve the reproducibility of the *FF*, as the statistical chart (**Figure S1,** ESI†) shows a narrower distribution of FF values in the 1D-ETL cells than in the mp-ETL cells. *FF* is significantly affected by the shunt and the series resistances. We attribute the higher and more reproducible FF to the better pore-filling with perovskite in the 1D-ETL, because incomplete pore-filling would increase the series resistance, and decrease the shunt resistance by the current leakage and the recombination due to the direct contact between the ETL and HTL and the exposure of ETL and light absorbing layer surfaces to air. Cross-sectional FE-SEM images (**Figure S2, ESI**) show that the mp-ETL cell has an appreciable amount of empty space after the perovskite formation, in contrast to the 1D-ETL cell.

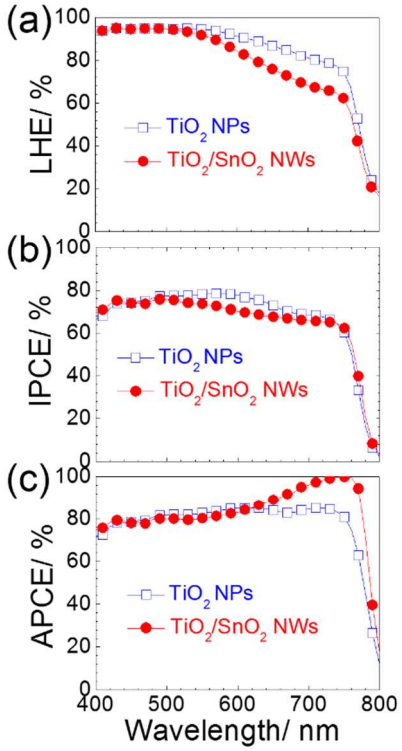

Figure 4. (a) LHE, (b) IPCE, and (c) APCE spectra of the TiO_2 NP-based mp-ETL and the TiO_2/SnO_2 NW-based 1D-ETL perovskite solar cells.

The relatively low J_{sc} can be understood as a result of the low light absorption property of the 1D-ETL cells. **Figure 4a** shows the light harvesting efficiency (LHE) of the ETL layers, calculated using the optical absorbance (A) and reflectance (R) shown in **Figure S3,** ESI†, as follows:[42]

$$LHE = (1-R)(1-10^{-A}) \quad (1)$$

Because the optical transmittance of SnO_2 NW/FTO is comparable to that of bare FTO, the low LHE of the 1D-ETL is attributed to small amount of the perovskite absorber material. Assuming hexagonally closed packed cylindrical nanowires,[17,43] the packing factor (PF), which is nanowire volume divided by geometric volume, is calculated to be ~0.9. On the other hand, PF of hexagonally closed packed spherical NPs is 0.74, which is the general fraction of volume in a hexagonal crystal structure. Therefore, the pore volume fraction of NP based ETL can be higher than NW based ETL, Considering that the thickness of perovskite/ETL layers are almost same for the both mp and 1D-ETL devices (see **Figure S2**, ESI†), the small absorber amount might be due to small pore volume of the 1D-ETL. The low LHE resulted in low external quantum yield (i.e. incident photon to current efficiency, IPCE) of 1D-ETL device, as shown in **Figure 4b**. The mp-ETL cell exhibits a slightly higher IPCE than the 1D-ETL cell especially in the wavelength range of 500 to 700 nm. However, it should be noted that, at long wavelengths (>700 nm), both cells show similar IPCE, in spite of the large

difference in LHE. To compare the internal quantum yields of the cells, the absorbed photon-to-current efficiency (APCE) was obtained from the IPCE and LHE as follows:

$$APCE = IPCE / LHE \quad (2)$$

Figure 4c shows that the APCE of the 1D-ETL reaches nearly 100% at the wavelength of 750 nm, implying the excellent electron-collection efficiency of 1D-ETL in longer wavelength regime.

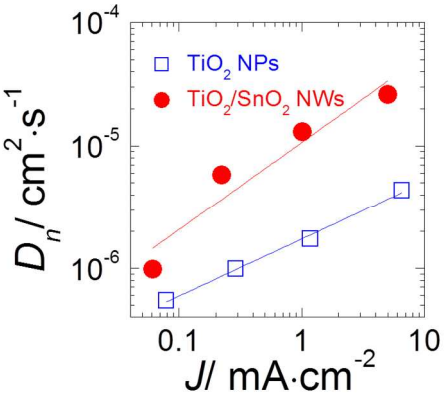

Figure 5. Electron diffusion coefficient of the TiO_2 NP-based mp-ETL perovskite solar cell, compared to the TiO_2/SnO_2 NW-based 1D-ETL perovskite solar cells.

The charge collection properties of the cells were investigated by measuring the electron diffusion coefficient, $D_n = t^2/(2.34\times\tau_n)$,[44] where t is thickness of the ETL layer and τ_n is the characteristic time constant of electron transport. **Figure 5** shows the 1D-ETL cell's D_n being about one order of magnitude greater than that of the mp-ETL cell, which is responsible for the extremely high internal quantum yield of the 1D-ETL cell. Several studies have reported faster electron transport in 1D-based dye-sensitized solar cells (DSSCs) compared to NP-based DSSCs,[45-47] while in perovskite solar cells D_n values for 1D versus NP structures have rarely been compared. We demonstrate here the enhanced electron transport in epitaxial 1D-ETL over that in NP-based mp-ETL. Therefore, it can be considered that the fast electron transport of the 1D-ETL compensates the IPCE, thus PCE, of the device, despite of its lower LHE than mp-ETL.

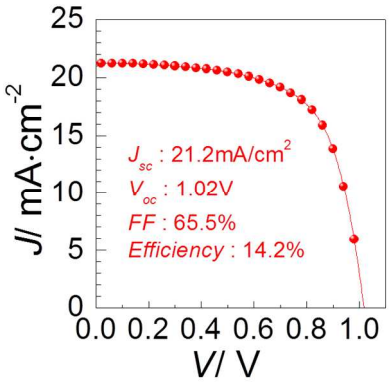

Figure 6. *J-V* curve for the best performing cell among the surface treated TiO_2/SnO_2 NW-based 1D-ETL perovskite solar cells.

Figure 6 shows the *J-V* curve of the best 1D-ETL cell, optimized by controlling the TiO_2/perovskite interfaces via $TiCl_4$ treatment. This cell exhibited PCE of 14.2%. The highly improved device performance is attributed to the $TiCl_4$ treatment which is well-known to modify the TiO_2 surface by increasing interconnection at the perovskite/TiO_2 interface and reducing the trap states of the TiO_2 surface.[48-51] We note that the high V_{oc} of 1.02 V, in spite of the lower conduction band edge of SnO_2 than that of TiO_2 by as much as 500 meV,[52,53] might be resulted from the passivation of recombination owing to the ALD TiO_2 thin layer, because SnO_2 layer without any passivation layer, such as TiO_2 or PbI_2, is known to exhibit very low V_{oc},[54,55] as also confirmed by our bare SnO_2 NW-based ETL PSC (Figure S4, ESI).

Conclusions

In summary, we demonstrated a 1D TiO_2-based perovskite solar cell which exhibits relatively high PCE, 14.2%, compared to other 1D-based perovskite solar cells. The 1D ETL layer is comprised of single-crystalline SnO_2 NWs as cores and epitaxial TiO_2 nanolayers as shells. The epitaxial TiO_2 rutile nanoshell enhanced electron transport compared to the conventional NP-based mp-ETL, which resulted in extremely high internal quantum yield more than 95% at around 750 nm of wavelength. Additionally, the open-pore structure led to excellent pore-filling with the perovskite material, considered to be the origin of the higher *FF* of the 1D-ETL cells compared to that of the mp-ETL cells. The optimized TiO_2/SnO_2 NW-based perovskite solar cell exhibited a high PCE of 14.2%, which is the best performance yet reported for 1D TiO_2 ETL-based perovskite solar cells.

Experimental

Preparation of electron transport layer

SnO_2 NWs were synthesized via the VLS reaction using a vapor transport method. Au seeds as the catalyst were coated over FTO substrate by using an ion beam coater. To grow SnO_2 nanowires, the Au/FTO substrate and tin powder were placed at the center of the tube furnace with some distance, under 700 ^oC in vacuum (1.0 mTorr) for 1.5 hr. Oxygen gas was flowed with a rate of 20 sccm into the tube furnace during the growth of SnO_2 NWs.

As the SnO_2 itself is not suitable for the ETL of perovskite solar cells because of its low conduction band edge (~-4.5 eV), TiO_2 nanoshell layer was employed for the ETL. TiO_2 nanoshell layers were deposited on the prepared SnO_2 NWs by using ALD method with the help of O_2 plasma, under 1.0 Torr of basial pressure at 300 ^oC.[9] After the deposition, TiO_2/SnO_2 NWs were annealed at 500 ^oC in air for 1h to achieve high crystallinity of TiO_2. We tested various thicknesses of TiO_2

nanoshells, and optimized the shell thickness of ~20 nm for efficient perovskite solar cells.

To compare the photovoltaic performance, TiO_2 NP-based mp-ETL was prepared following the methods reported previously.[56] First, compact TiO_2 layer was deposited on FTO substrate. A titanium diisopropoxide bis(acetylacetonate) solution (in 1-butanol, 0.15 M) was coated on an FTO substrate, and dried at 120 ^oC for 10 min. Then 0.3 M titanium diisopropoxide bis(acetylacetonate) solution was coated onto the substrate using the same method. After then the substrate was annealed at 500 ^oC for 15 min. After cooling to room temperature, the substrate was immersed in $TiCl_4$ solution (aqueous, 0.05 M) for 30 min at 70 ^oC. Then the substrates were rinsed with deionized (DI) water several times, and annealed at 500 ^oC for 15 min. Second, TiO_2 mesoporous layer was formed on the prepared substrate, using TiO_2 NPs (~20 nm, 18NRT)-based paste purchased from Dyesol^{TM}. A diluted paste (in ethanol, 1:3.5 wt%) was spin-coated onto the $TiCl_4$-treated substrate, and then annealed at 500 ^oC in air for 45 min.

Fabrication of Perovskite Solar Cells

The light absorbing perovskite layer was coated on the prepared ETL by the sequential deposition of PbI_2 and methyl ammonium iodide (MAI, CH_3NH_3I).[56] MAI was prepared according to the reported procedure.[5] 30 mL of hydriodic acid (57 wt% in water) was stirred on a round bottom flask with 27.8 mL of methylamine (40% in methanol) at 0 ^oC for 2 hr. Then, the solution was evaporated to precipitate the MAI. The MAI was washed three times in diethyl ether, and dried at 60 ^oC in vacuum oven for 6 hr. The prepared ETLs were coated with a PbI_2 solution (1.0 M, in dimethylformamide), and dried at 70 ^oC. Then, they were dipped in an MAI solution (10 $mg{\cdot}mL^{-1}$, in 2-propanol) for 60 sec, rinsed with 2-propanol, and dried at 70 ^oC for 30 min.

HTL was deposited on the perovskite layer by spin-coating (4000 rpm, 40 sec) spiro-OMeTAD (2,2'7,7'-tetrakis-(N,N-dipmethoxyphenylamine) 9,9'-spirobifluorene) -based solution. The solution was prepared by dissolving spiro-OMeTAD (72 mg) in chlorobenzene (1 mL), with adding 4-tert-butylpyridine (28.8 μL) and lithium-bis(trifluoro-methanesulphonyl)imide salt (17.6 μL, 520 $mg{\cdot}mL^{-1}$ in acetonitrile). Finally, 80 nm-thick Ag electrodes were deposited on HTM layers via using thermal evaporation.

Device Characterization

Microstructures of the 1D-ETLs and devices were analyzed by using a field-emission scanning electron microscopy (FESEM, JSM-7600F, JEOL) and HR-TEM (JEM-2100F, JEOL). Optical transmittance and absorbance of the materials were measured by using an UV/vis spectrometer (PerkinElmer). Crystal structures were analyzed by using Raman spectroscopy (WITec alpha 300M), and SAED combined with the HRTEM. Photovoltaic performances were evaluated using a potentiostat (CHI660, CHI instrument), under the global AM 1.5 condition simulated by a solar simulator (Oriel Sol 3A class AAA, Newport). Active cell area was 0.14 cm^2. Photocurrent density–voltage (*J-V*) curves were collected with 0.05 $V{\cdot}sec^{-1}$ of scan rate. Time constant for photo-generated electron transport (τ_n) was measured using a transient photocurrent–voltage spectroscopy setup, which is described elsewhere.[56] The incident photon-to-current conversion efficiency (IPCE) was measured using a monochromatic light grating system (PV Measurements).

Acknowledgements

This work was supported by the National Research Foundation of Korea (NRF) grants funded by the Ministry of Science, ICT & Future Planning (MSIP) of Korea under contracts no. NRF-2014R1A4A1008474, 2012M3A7B4049967 (Nano . Material Technology Development Program) and 2012M3A6A7054855 (Global Frontier R&D Program on Center for Multiscale Energy System).

Notes and references

[a] School of Advanced Materials Science & Engineering, Sungkyunkwan University, Suwon 440-746, Republic of Korea.
[b] Department of Mechanical Engineering & Materials Science, University of Pittsburgh, PA15261, USA
[c] Department of Materials Science and Engineering, Seoul National University, Seoul 151-744, Republic of Korea
[d] School of Chemical Engineering and Department of Energy Science, Sungkyunkwan University, Suwon, 440-746, Republic Korea.
[e] Department of Materials Science and Engineering, Ajou University, Suwon 443-749, Korea
[f] Department of Material Science and Engineering, University of California at Berkeley, CA94720, USA.

† Electronic Supplementary Information (ESI) available: Histograms of the parameters, UV-vis absorption spectrum and the cross-sectional FE-SEM image of the TiO_2 NP based mp-ETL cell, TiO_2/SnO_2 NWs based 1D-ETL perovskite solar cells and exposure FTO at grown SnO_2 NWs on FTO substrate.

See DOI: 10.1039/b000000x/

1 N. –G. Park, *J. Phys. Chem. Lett.*, 2013, **4**, 2423.
2 H. J. Snaith, *J. Phys. Chem. Lett.*, 2013, **4**, 3623.
3 H. –S. Kim, C. –R. Lee, J. –H. Im, K. –B. Lee, T. Moehl, A. Marchioro, S.-J. Moon, R. Humphry-Baker, J.-H. Yum, M. Grätzel, *Sci. Rep.*, 2012, **2**, 591.
4 J. H. Heo, S. H. Im, J. H. Noh, T. N. Mandal, C.-S. Lim, J. A. Chang, Y. H. Lee, H. J. Kim, A. Sarkar, M. K. Nazeeruddin, M. Grätzel, S. I. Seok, *Nat. Photonics*, 2013, **7**, 486.
5 M. M. Lee, J. Teuscher, T. Miyasaka, T. N. Murakami and H. J. Snaith, *Science*, 2012, **338**, 643.
6 J. H. Noh, S. H. Im, J. H. Heo, T. N. Mandal, S. I. Seok, *Nano Lett.*, 2013, **13**, 1764.
7 D.-Y. Son, J.-H. Im, H.-S. Kim, N.-G. Park, *J. Phys. Chem. C*, 2014, **118**, 16567.

8 D.-Y. Son, K. –H. Bae, H. –S. Kim, N. –G. Park, *J. Phys. Chem. C* 2015, **119**, 10321.
9 G. S. Han, S. Lee, J. H. Noh, H. S. Chung, J. H. Park, B. S. Swain, J.-H. Im, N.-G. Park, H. S. Jung, *Nanoscale*, 2014, **6**, 6127.
10 J. T. -W. Wang, J. M. Ball, E. M. Barea, A. Abate, J. A. Alexander-Webber, J. Huang, M. Saliba, I. Mora-Sero, J. Bisquert, H. J. Snaith, R. J. Nicholas, *Nano Lett.*, 2014, **14**, 724.
11 W. S. Yang, J. H. Noh, N. J. Jeon, Y. C. Kim, S. Ryu, J. Seo, S. I. Seok, *Science*, 2015, **348**, 6240.
12 H. –S. Kim, S. H. Im, N. –G. Park, *J. Phys. Chem. Lett.*, 2014, **118**, 5615.
13 L. Schmidt-Mende and M. Grätzel, *Thin Solid Films*, 2006, **500**, 296
14 Fraas, L. M. *J. Appl. Phys.*, 1978, **49**, 871–875.
15 J.-H. Im, I.-H. Jang, N. Pellet, M. Grätzel and N.-G. Park, *Nat. Nanotechnol.*, 2014, **9**, 927
16 H. J. Snaith, R. Humphry-Baker, P. Chen, I. Cesar, S. M. Zakeeruddin, M. Grätzel, *Nanotechnology*, 2008, **19**, 424003.
17 H.-S. Kim, J.-W. Lee, N. Yantara, P. P. Boix, S. A. Kulkarni, S. Mhaisalkar, M. Grätzel and N.-G. Park, *Nano Lett.*, 2013, **13**, 2412.
18 D. Bi, G. Boschloo, S. Schwarzmüller, L. Yang, E. M. J. Johanssona, A. Hagfeldt, *Nanoscale*, 2013, **5**, 11686.
19 S. Lee, I. J. Park, D. H. Kim, W. M. Seong, D. W. Kim, G. S. Han, J. Y. Kim, H. S. Jung and K. S. Hong, *Energy Environ. Sci.*, 2012, **5**, 7989
20 J. Dong, Y. Zhao, J. Shi, H. Wei, J. Xiao, X. Xu, J. Luo, J. Xu, D. Li, Y. Luo, Q. Meng, *Chem. Commun.*, **2014**, 50, 13381.
21 J. Zhang, P. Barboux, T. Pauportè, *Adv. Energy Mater.,* 2014, **4**, 1400932.
22 S. S. Mali, C. S. Shim, H. J. Park, J. Heo, P. S. Patil, C. K. Hong, *Chem. Mater.*, 2015, **27**, 1541.
23 D. Liu, T. L. Kelly, *Nature Photonics*, 2014, **8**, 133
24 X. Zhang, Z. Bao, X. Tao, H. Sun, W. Chen, X. Zhou, *RSC Advances*, 2014, **4**, 64001
25 M. Yang, R. Guo, K. Kadel, Y. Liu, K. O'Shea, R. Bone, X. Wang, J. He, W. Li, *J. Mater. Chem. A*, 2014, **2**, 19616.
26 D. Zhong, B. Cai, X. Wang, Y. Xing, S. Miao, W. –H. Zhang, C. Li, *Nano Energy*, 2015, **11**, 409.
27 B. Cai, D. Zhong, Z. Yang, B. Huang, S. Miao, W. –H. Zhang, J. Qiu, C. Li, *J. Mater. Chem. C*, 2015, **3**, 729.
28 S. J. Ku, G. C. Jo, C. H. Bak, S. M. Kim, Y. R. Shin, K. H. Kim, S. H. Kwon, J. –B. Kim, *Nanotechnology*, 2013, **24**, 085301
29 Q. Wei, K. Hirota, K. Tajima, K. Hashimoto, *Chem. Mater.*, 2006, **18**, 5080.
30 Y. J. Hwang, C. Hahn, B. Liu, P. Yang, *ACS NANO*, 2012, **6**, 5060
31 H. S. Chung, G. S. Han, S. Y. Park, H. –W. Shin, T. K. Ahn, S. Jeong, I. S. Cho, H. S. Jung, *ACS Appl. Mater. Interfaces*, 2015, DOI: 10.1021/acsami.5b00948.
32 I. S. Cho, Z. Chen, A. J. Forman, D. R. Kim, P. M. Rao, T. F. Jaramillo, X. Zheng, *Nano Lett.*, 2011, **11**, 4978.
33 R. S Wagner, C. J. Doherty, *J. Electrochem. Soc.*, 1968, **115**, 93.
34 A. Kar, M. A. Stroscio, M. Dutta, M. Meyyappan, *Phys. Status Solidi B*, 2011, **248**, 12, 2848.
35 S. Park, S. –D. Seo, S. Lee, S. W. Seo, K. –S. Park, C. W. Lee, D. -W. Kim, K. S. Hong, *J. Phys. Chem. C*, 2012, **116**, 21717.
36 A. M. Nie, J. B. Liu, Q. Q. Li, Y. C. Cheng, C. Z. Dong, W. Zhou, P. Wang, Q. X. Wang, Y. Yang, Y. H. Zhu, Y. W. Zeng, H. T. Wang, *J. Mater. Chem.*, 2012, **22**, 10665.
37 J. Yan, G. Wu, N. Guan, L. Li, Z. Li, X. Cao, *Phys.Chem. Chem. Phys.*, 2013, **15**, 10978.
38 H. T. Wang, S. Xu and R. G. Gordon, *Electrochemical and Solid State Letters*, 2010, **13**, G75.
39 S. K. Kim, W. D. Kim, K. M. Kim, C. S. Hwang and J. Jeong, *Appl. Phys. Lett.*, 2004, **85**, 4112.
40 S. K. Kim, G. W. Hwang, W. D. Kim and C. S. Hwang, *Electrochemical and Solid State Letters.*, 2006, **9**, F5.
41 M. Schuisky, A. Harsta, A. Aidla, K. Kukli, A. A. Kiisler and J. Aarik, *J. Electrochem. Soc.*, 2000, **147**, 3319.
42 A. G. Agrios, A. Hagfeldt, *J. Phys. Chem. C*, 2008, **112**, 10021.
43 A. B. F. Martinson, J. W. Elam, J. T. Hupp, M. J. Pellin, *Nano Lett.*, 2007, **7**, 2183-2187.
44 J. van de Lagemaat, A. J. Frank, *J. Phys. Chem. B*, 2001, **105** (45), 11194.
45 J. H. Noh, H. S. Han, S. Lee, J. Y. Kim, K. S. Hong, G. S. Han, H. Shin and H. S. Jung, *Adv. Energy Mater.*, 2011, **1**, 829.
46 M. Wang, J. Bai, F. L. Formal, S. -J. Moon, L. Cevey-Ha, R. Humphry-Baker, C. Grätzel, S. M. Zakeeruddin and M. Grätzel, *J. Phys. Chem. C*, 2012, **116**, 3266
47 K. Zhu, N. R. Neale, A. Miedaner and A. J. Frank, *Nano Lett.*, 2007, **7**, 69.
48 A. Fakharuddin, F. D. Giacomo, I. Ahmed, Q. Wali, T. M. Brown b, R. Jose, *Journal of Power Sources*, 2015, **283**, 61–67
49 I. Ahmed, A. Fakharuddin, Q. Wali, A.R. Zainun, J. Ismail, R. Jose, *Nanotechnology*, 2015, **26**, 105401.
50 P.M. Sommeling, B.C. O'Regan, R.R. Haswell, H.J.P. Smit, N.J. Bakker, J.J.T. Smits, J.M. Kroon, J.A.M. van Roosmalen, *J. Phys. Chem. B*, 2006, **110**, 19191-19197.
51 A. Yella, L.P. Heiniger, P. Gao, M.K. Nazeeruddin, M. Grätzel, *Nano Lett.*, 2014, **14**, 2591-2596.
52 A. Imanish, E. Tsuji, Y. Nakato, *J. Phys. Chem. C*, 2007, **111**, 2128.
53 M. Batzill, U. Diebold, *Progress in Surface Science,* 2005, **79**, 47.
54 Z. Zhu, X. Zheng, Y. Bai, T. Zhang, Z Wang, S. Xiao, S. Yang, *Phys.Chem.Chem.Phys*., 2015, **17**, 18265
55 J. Song, E. Zheng, J. Bian, X. –F. Wang, W. Tian, Y. Sanehirac, T. Miyasakac, *J. Mater. Chem. A*, 2015, **3**, 10837.
56 J. Burschka, N. Pellet, S. J. Moon, R. Humphry-Baker, P. Gao, M. K. Nazeeruddin, M. Grätzel, *Nature*, 2013, **499**, 316.
55 M. J. Kim, C. R. Lee, W. S. Jeong, J. H. Im, T. I. Ryu and N. –G. Park, *J. Phys. Chem. C*, 2010, **114**, 19849.

